RSC Advances

PAPER

View Article Online
View Journal | View Issue

Cite this: *RSC Adv.*, 2020, **10**, 15264

Hybrid fluorescent liquid crystalline composites: directed assembly of quantum dots in liquid crystalline block copolymer matrices†

Miron Bugakov, *[a] Sharifa Abdullaeva,[a] Pavel Samokhvalov,[b] Sergey Abramchuk,[ac] Valery Shibaev[a] and Natalia Boiko[a]

Received 16th March 2020
Accepted 3rd April 2020

DOI: 10.1039/d0ra02442b

rsc.li/rsc-advances

Hybrid fluorescent liquid crystalline (LC) composites containing inorganic quantum dots (QDs) are promising materials for many applications in optics, nanophotonics and display technology, combining the superior emission capability of QDs with the externally controllable optical properties of LCs. In this work, we propose the hybrid LC composites that were obtained by embedding CdSe/ZnS QDs into a series of host LC block copolymers of different architectures by means of a two-stage ligand exchange procedure. The ABA/BAB triblock copolymers and AB diblock copolymers with different polymerization degrees are composed of nematogenic phenyl benzoate acrylic monomer units and poly(4-vinylpyridine) blocks, which are capable of binding to the QD surface. Our results clearly show that the spatial distribution of QDs within composite films as well as the formation of QD aggregates can be programed by varying the structure of the host block copolymer. The obtained composites form a nematic LC phase, with isotropization temperatures being close to those of the initial host block copolymers. In addition, the influence of the molecular architecture of the host block copolymers on fluorescence properties of the obtained composites is considered. The described strategy for the QD assembly should provide a robust and conventional route for the design of highly ordered hierarchical hybrid materials for many practical applications.

Introduction

Hybrid fluorescent polymer composites are of great scientific and technological interest as a new generation of materials for nanophotonics,[1–3] sensing,[4,5] optical coding,[6] and display technology.[7,8] These composites offer a unique opportunity for design and development of new hybrid systems by combining the features of both organic and inorganic components in one material. Fluorescence properties of these composites are usually provided by the inorganic part – semiconductor nanocrystals, such as quantum dots (QDs), nanorods or nanoplatelets. QDs are well-known for their unique fluorescence properties such as size-dependent emission, high optical stability, high fluorescence quantum yield and emission brightness.[9,10] The second component of the hybrid material, the polymer matrix, is responsible for the mechanical properties of the composite and allows fabrication of films or fibers.[11–14] Besides that, the polymer matrix can stabilize QDs, pattern them or provide some extra functionality of the hybrid material if a specialized polymer is used as the matrix.

Liquid crystalline (LC) polymers may be considered as a promising functional polymer matrix for hybrid fluorescent polymer composites with externally controllable emission. LC polymers combine good processing properties of polymers with the features of an LC phase: anisotropy, self-assembly and sensitivity to a broad range of external factors. Following these considerations, successful attempts to incorporate QDs in LC homopolymers and random copolymers have been reported.[15–18] Depending on the type of the LC phase, the obtained composites were found to exhibit various optical and morphological features. Thus, in the hybrid films of smectic LC polymers QDs were assembled in thin layers, and alternate nanolayers of LC polymer and nanoparticles were observed.[15] Introducing QDs into cholesteric LC polymers allowed materials with photooptically and electrically controlled circularly polarized fluorescence to be designed.[16]

Although some success has been reached in the preparation of hybrid LC composites, there is one crucial challenge lying in intrinsic incompatibility between the QDs and LC polymer matrix. Generally, the LC phase prefers to force out nanoparticles, which are compelled to form aggregates or

[a]*Department of Chemistry, Moscow State University, Leninskie Gory-1, 119991, Moscow, Russian Federation. E-mail: miron.bugakov@vms.chem.msu.ru*

[b]*Laboratory of Nano-Bioengineering, National Research Nuclear University MEPhI (Moscow Engineering Physics Institute), 115522 Moscow, Russia*

[c]*Nesmeyanov Institute of Organoelement Compounds, Russian Academy of Sciences, Moscow, 119991, Russia*

† Electronic supplementary information (ESI) available: ^{1}H NMR spectra, TEM, and fluorescence spectroscopy data. See DOI: 10.1039/d0ra02442b

accumulate in the defects of an LC phase.[19,20] This reason limits the maximum allowable concentration of QDs in hybrid LC composites and may provoke a macrophase separation. The problem of phase incompatibility could be overcome by using LC homopolymers and random copolymers, which contain special "anchor" monomer units suitable for attaching to the QD surface.[15,18] Such an approach can considerably decrease the aggregation of QDs, thus allowing to prepare LC composites with QD content up to 20 wt%. However, some unevenness of the QD distribution still can be detected in the obtained composites. Moreover, introducing QDs directly into the LC phase may disturb an LC order and result in alteration of the characteristics of the LC phase. As it has been shown in ref. 15, introducing QDs into the LC phase can decrease the melting point of the latter and increase the glass transition temperature of composites. In turn, these effects can result in the contraction of the temperature range of the LC phase formation.

An alternative approach to achieve better compatibility between inorganic nanoparticles and organic matrix is based on the application of block copolymers containing a block capable of binding to nanoparticle surface. By this approach, many hybrid QD composites have been prepared[21–24] and various photonic elements including 3D photonic array containing QDs,[25] multi-color emitting hybrid microspheres,[26] electroluminescent films,[27] hybrid organic films for solar cells,[28] hybrid nanowires,[29] and resonators for microcavity lasing[30] have been demonstrated. In addition to good compatibility between nanoparticles and a polymer matrix, block copolymers furnish excellent opportunity to develop a multifunctional polymer matrix for hybrid composites due to the following reasons.

Block copolymers, as a rule, are characterized by microphase separated structure where each constituent block forms its own microphase. Lamellar, cylindrical, gyroid, spherical and many other structures have been observed in block copolymer materials.[31–34] The specific type of the structure formed by a block copolymer is defined by the ratio between its constituent blocks, their sequence and chemical structure. The presence of such microstructure in the hybrid composite film provokes accumulation of QDs in the microphases of the binding block, thus leading to self-assembly of QDs in various three-dimensional arrangements.[24,35] Furthermore, one or more blocks of a block copolymer can include particular functional units that endow composites with specific functions. Using this approach, conducting QD/polymer hybrid films with good processability and film formation properties were prepared.[36] These films were manifested as an efficient material for light-emitting diodes in comparison with pristine QDs. It should be stressed that the specific functional groups may be localized in microphases that do not contain QDs if the interaction between QDs and such groups is undesirable.

In view of the foregoing, LC block copolymers containing a block capable of binding to QDs could be a convenient and versatile platform for designing hybrid LC–QD composites with controllable spatial distribution of QDs. Nevertheless, to our knowledge, there has been no report that is devoted to such hybrid composites prepared on the basis of LC block copolymers and QDs. In our recent report we have tested ABA LC triblock copolymers containing two end poly(4-vinylpyridine) blocks as the host matrix for hybrid fluorescent LC polymer–QD composites.[37] The aim of that work was to achieve a significant concentration of QDs embedded into the polymer matrix while keeping their dispersion stable. We have demonstrated that these block copolymers allow preparation of composites with the loading of QDs up to 10 wt%. The obtained composites are characterized by the uniform QD distribution and complete preservation of the characteristics of pristine LC phase.

Here, our motivation is to study the influence of the LC block copolymer molecular architecture on the morphology of LC polymer–QD composite films in terms of spatial distribution and assembly of QDs. In addition, phase behavior and fluorescence properties of the hybrid composites are examined.

To achieve this, we synthesized a series of LC block copolymers that enabled us to trace the effects of three parameters of the block copolymer architecture (Fig. 1a) on the morphology of LC–QD composites. These parameters include (i) the number of blocks in a copolymer (tri- and diblock copolymers), (ii) the mutual arrangement of blocks (ABA and BAB triblock copolymers), and (iii) the polymerization degree of LC and poly(4-vinylpyridine) blocks (pVP blocks). In addition, we compared these block copolymers with random copolymers having the same ratio of monomer units from the standpoint of their applicability as a matrix of hybrid LC composites. Our LC block copolymers are composed of acrylic phenyl benzoate (PhM) monomer units forming a nematic LC phase, and pVP blocks capable of binding to QDs. PhM block forming only the simplest nematic LC phase[38] was chosen as an LC part of the block copolymers to focus on morphology of hybrid composites. The choice of VP units for a binding block is associated with the high ability of poly(4-vinylpyridine) to bind to the QD surface.

Results and discussion

Composite preparation

All copolymers used in this work were synthesized by the reversible addition fragmentation chain transfer (RAFT) polymerization. The symmetrical ABA (A and B stand for PhM and pVP blocks, respectively) triblock copolymers with end pVP blocks were obtained according to the procedure described previously (Scheme S1†).[39] The same procedure was used for the BAB triblock and diblock copolymers but the polymerization processes were mediated by two other RAFT agents. The diblock copolymers were synthesized in the presence of commercially available CPDDTC (Fig. S1a†), containing one trithiocarbonate fragment. In the case of the BAB triblock copolymer, a special RAFT agent was synthesized (Fig. S1b†) using the modified procedure described in the literature.[40] This RAFT agent named as di-CPDDTC contains two trithiocarbonate fragments leaving groups of which are connected by a small spacer. The use of di-CPDDTC agent allowed us to keep the sequence of the monomer addition as it was done in the case of the synthetic procedure described for the ABA triblock copolymers. The sequence of the monomer addition is important because the activity of 4-vinylpyridine in copolymerization with alkyl acrylates is higher by more than an order of magnitude.[41,42] The random

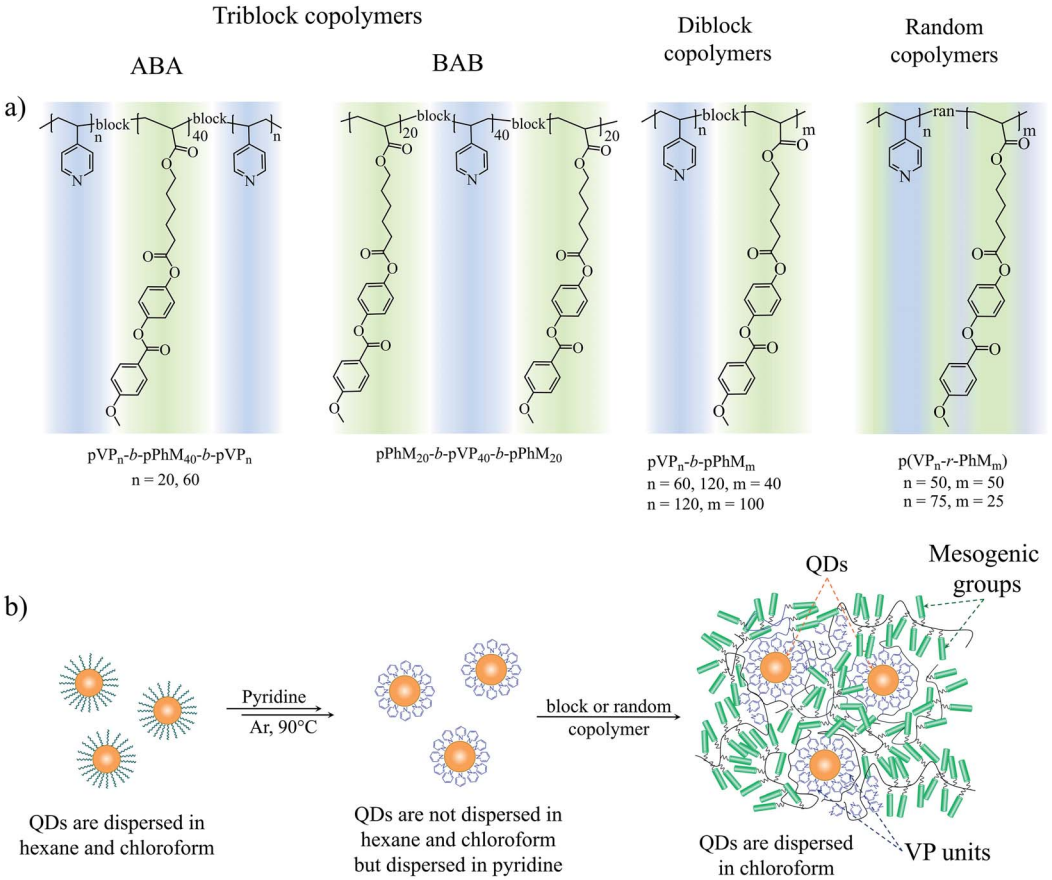

Fig. 1 (a) The chemical structure of the triblock, diblock and random copolymers. (b) The schematic route of the ligand exchange procedure.

copolymers were synthesized in the presence of CPDDTC, but both PhM and VP monomers were added simultaneously.

The chemical structures of all the copolymers were analyzed and proved by ^{1}H NMR spectroscopy and gel permeation chromatography (GPC). Molecular weights and polydispersity indices (PDI) of all the copolymers are presented in Table S1.†

The CdSe/ZnS QDs that were used in our study were synthesized according to the previously reported procedure.[43] The QDs were approximately 5 nm in diameter and contained oleylamine (OLA) surfactant on their surface as a ligand.

The LC polymer–QD composites were prepared by a two-step ligand exchange procedure described in our previous paper.[37] QDs initially capped with OLA were treated with pyridine three times, and then the labile pyridine ligands were exchanged for polymer ligand bearing the same binding groups, a block copolymer or a random copolymer. Each stage of the ligand exchange was confirmed by the change in solubility of QDs in the respective solvent (Fig. 1b). Thus, after the first ligand exchange QDs covered with pyridine became insoluble in hexane or chloroform. When pyridine molecules were substituted with pVP blocks or units of the copolymer, their solubility in chloroform was restored. Additionally the presence of pyridine on the surface of QDs was confirmed by ^{1}H NMR (Fig. S2†) and FTIR (Fig. 2) spectroscopy. As can be seen, both methods evidence the presence of aromatic compounds: the peaks between 8.68 and 7.17 ppm in the ^{1}H NMR spectrum and peaks at 1069, 1448, 1113, 1045 and 696 cm^{-1} in the FTIR spectrum. It is important to note that the peaks associated with the alkyl chain of oleylamine are still present in both ^{1}H NMR and FTIR spectra. However, as it will be discussed in the following sections, the achieved degree of ligand exchange is

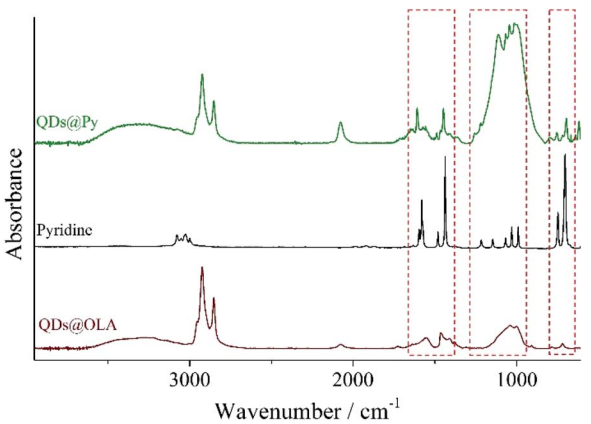

Fig. 2 FTIR spectra of pyridine, QDs coated with oleylamine (QDs@OLA) and QDs after the ligand exchange procedure (QDs@Py). Dashed rectangles mark spectral areas where characteristic peaks of pyridine are present.

enough for the successful preparation of the LC polymer–QD composites.

We suppose that the replacement of pyridine ligands by pVP blocks of block copolymers is promoted by the following factors. First of all, this process can be considered as entropy-driven due to the release of small pyridine molecules. Further on, the pVP block of the copolymers is a polydentate ligand and its complexation to the QD surface should be much stronger than that of monodentate pyridine. Finally, pyridine is a volatile substance that can be easily removed under reduced pressure so that the exchange equilibrium is shifted towards the formation of the complex with the copolymer.

As a result of the two stage ligand exchange procedure describe above, we have obtained a series of LC polymer–QD composites, which differ in the type of the copolymer ligand but have the same loading of QDs equal to 10 wt% (Table 1). The LC polymer–QD composites were designated according to the chemical structure of the host polymer matrix. For instance, the composites based on the ABA triblock copolymers are marked as V_n-LC_m-V_n, while the composites based on the AB diblock copolymer are marked as V_n-LC_m. In all cases, *n* and *m* stand for the polymerization degree of pVP and PhM blocks respectively. Since the loading of QDs in all of the composites was equal to 10 wt%, it was not reflected in the designation of composites.

Phase behavior and morphology of the copolymers

Before discussing the characteristics of the hybrid composites, the phase behavior and morphology of the host LC block and random copolymers should be considered. As it was determined by POM, all the block copolymers form a nematic LC phase with a marble texture that is typical of the PhM homopolymer (Fig. 3a). However, there is the difference in isotropization temperatures of the block copolymers (Table S2†) that may be explained by the following reasons. As it was reported previously, the isotropization temperature of PhM homopolymer depends on the length of its polymer chain in the case when the polymerization degree is lower than 100.[38] This could explain the changes in the isotropization temperature within the series of diblock and triblock copolymers. Furthermore, the lower isotropization temperature of the triblock copolymers when compared to the diblock copolymers may be associated with the confinement of PhM units between two amorphous pVP blocks in the former. This confinement may increase the number of defects in the ordering of PhM groups near the microphase interfaces and, as a result, decrease the isotropization temperature of nematic phase. In contrast to block copolymers, the random copolymers with the same ratio of monomer units did not form any LC phase.

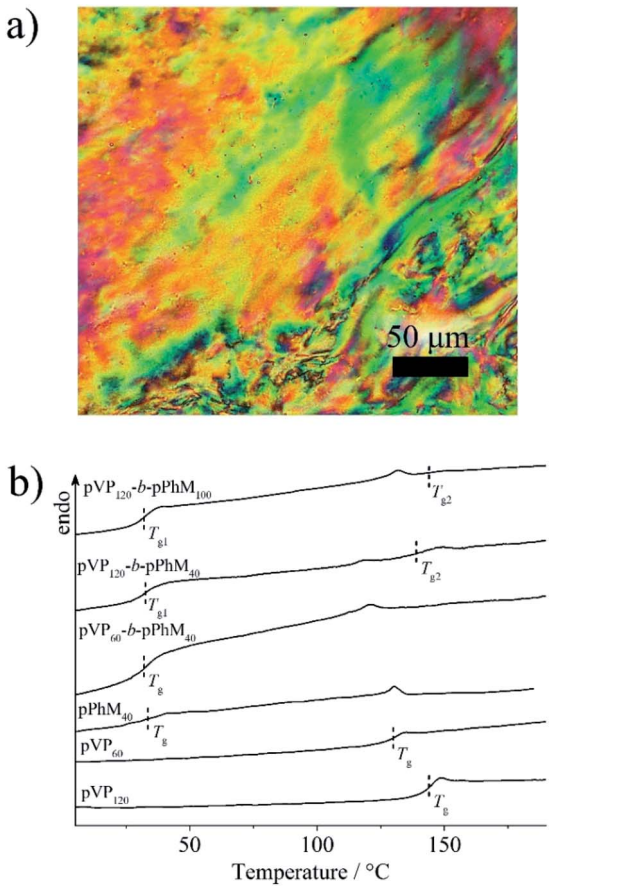

Fig. 3 (a) The POM images of the pVP_{120}-*b*-$pPhM_{100}$ sample and (b) DSC curves of the diblock copolymers and homopolymers.

DSC measurements have revealed that pVP_{120}-*b*-$pPhM_{100}$ and pVP_{120}-*b*-$pPhM_{40}$ diblock copolymers have two glass

Table 1 Phase behavior and morphology of the hybrid composites

Composite	Host copolymer	Glass transition temperature, °C	Phase behavior[a]	Microphase separation[b]
V_{20}-LC_{40}-V_{20}	pVP_{20}-*b*-$pPhM_{40}$-*b*-pVP_{20}	33	N 105 (0.6) I	U
V_{60}-LC_{40}-V_{60}	pVP_{60}-*b*-$pPhM_{40}$-*b*-pVP_{60}	34	N 111 (0.3) I	L
LC_{20}-V_{40}-LC_{20}	$pPhM_{20}$-*b*-pVP_{40}-*b*-$pPhM_{20}$	30	N 87 (0.6) I	U
V_{120}-LC_{100}	pVP_{120}-*b*-$pPhM_{100}$	32	N 127 (0.6) I	C
V_{120}-LC_{40}	pVP_{120}-*b*-$pPhM_{40}$	32/138	N 117 (0.2) I	L
V_{60}-LC_{40}	pVP_{60}-*b*-$pPhM_{40}$	31	N 115 (0.7) I	U
VLC-1	p(VP_{50}-*r*-$pPhM_{50}$)	50	—	—
VLC-2	p(VP_{75}-*r*-$pPhM_{25}$)	67	—	—

[a] N – nematic phase, I – isotropic melt. Isotropization enthalpy (in J g^{-1}) is given in brackets. [b] L – lamellar structure, C – cylindrical structure, and U – unclear type of a microphase separated structure, which still contains discrete microphases formed by pVP blocks.

transition points (Fig. 3b, Table S2†). The one of them located near 31 °C could be assigned to the PhM block while the higher value is close to that of the VP block. The rest of the block copolymers are characterized by only one glass transition temperature, which is approximately 32 °C and can be associated with the PhM block. The glass transition temperatures of the p(VP_{50}-*r*-pPhM_{50}) and p(VP_{75}-*r*-pPhM_{25}) random copolymers were found to be 51 and 65 °C, respectively, that is, their physicochemical properties are additive.

The presence of two glass transition temperatures in the DSC curve of a block copolymer is an indirect indication that the microphase separation occurs in the polymer structure. To reveal the microphase separation structure, thin slices of block copolymer samples were studied with TEM. The TEM samples were stained with iodine to increase the contrast between pVP and PhM microphases. As it has been shown previously,[44] iodine molecules are selectively adsorbed by pyridine groups and dark areas in TEM images thus correspond to microphases formed by pVP blocks.

The TEM study of the pVP_{120}-*b*-pPhM_{40} and pVP_{120}-*b*-pPhM_{100} films revealed the formation of lamellar and cylindrical structures, respectively (Fig. 4a and b). These types of microphase separated structures agree well with the weight fraction of the monomer units in these diblock copolymers (Table S1†). According to the Fourier-transform (FT) analysis, the pVP_{120}-*b*-pPhM_{40} film is characterized by well-ordered lamellar structure with the mean microphase spacing of about 18 nm. Note that the FFT image of the pVP_{120}-*b*-pPhM_{40} film (inset in Fig. 4a) displays the second-order peaks and this is the evidence of high order of the lamellar structure. This highly ordered structure is supposed to result from the interplay between the microphase separation and the LC elastic deformation.[45] The pVP_{120}-*b*-pPhM_{100} film showed a cylindrical microphase structure with the diameter of cylinders of about 12 nm and the cylinder-to-cylinder distance about 20 nm. The FFT image of the pVP_{120}-*b*-pPhM_{100} film indicates the preferential hexagonal packing of cylinders. The hexagon has a slightly oblate shape, which is likely due to the distortion of the film with a diamond knife during the sample preparation.

In the case of pVP_{60}-*b*-pPhM_{40}, the character of the microphase separated structure could not be clearly identified from TEM image (Fig. S3†). This is likely to be due to the relatively low polymerization degree of this copolymer. The FFT pattern indicates the mean feature spacing of 13 nm for the pVP_{60}-*b*-pPhM_{40} film without any long-range order. The pVP_{60}-*b*-pPhM_{40} block copolymer is characterized by almost the same ratio between the pVP and PhM monomer units as pVP_{120}-*b*-pPhM_{100}, which forms cylindrical microphase structure. However, the polymerization degree of pVP_{60}-*b*-pPhM_{40} is lower and this could lead to the transit of this block copolymer to a disorder area in the phase diagram of such system.[46] Thus, the structure of pVP_{60}-*b*-pPhM_{40} may be considered as a disordered inclusion of short cylindrical or spherical microphases formed by the pVP blocks into the host matrix.

The pVP_{60}-*b*-pPhM_{40}-*b*-pVP_{60} film displayed a lamellar structure with the spacing of 15 nm (Fig. 4c), although only one glass transition temperature could be resolved in the DSC curve. The lamellar structure of the pVP_{60}-*b*-pPhM_{40}-*b*-pVP_{60} film was less ordered in comparison with that of the pVP_{120}-*b*-pPhM_{40} film. This fact may be associated with two possibilities. First, the triblock copolymers have two junction points connecting different blocks as opposed to diblock copolymers having only one junction point. As junction points prefer to be located at the interfaces between the microphases,[47] the whole macromolecules of a block copolymer are forced to be packed in an appropriate spatial arrangement. Thus, in the case of a diblock copolymer only one junction point should be settled at the interface, what could be easily realized as a regular lamellar, cylindrical or another microstructure. On the other hand, the macromolecules of a triblock copolymer have to arrange two junction points on the boundary between microphases. Therefore, the packing of macromolecules of triblock copolymer looks more difficult and may provoke a considerable decrease in entropy. To compensate for this, a lamellar structure without a long-range order may be formed. It is corroborated with the fact that the pVP_{60}-*b*-pPhM_{40}-*b*-pVP_{60} film demonstrates a perfectly oriented lamellar structure near the PET substrate. In addition, some ordering impediment of the LC phase on the microphase separation may occur due to the constraints of the PhM block caused by end pVP blocks.

An undefined microphase separated structure was observed for the pVP_{20}-*b*-pPhM_{40}-*b*-pVP_{20} and pPhM_{20}-*b*-pVP_{40}-*b*-pPhM_{20}

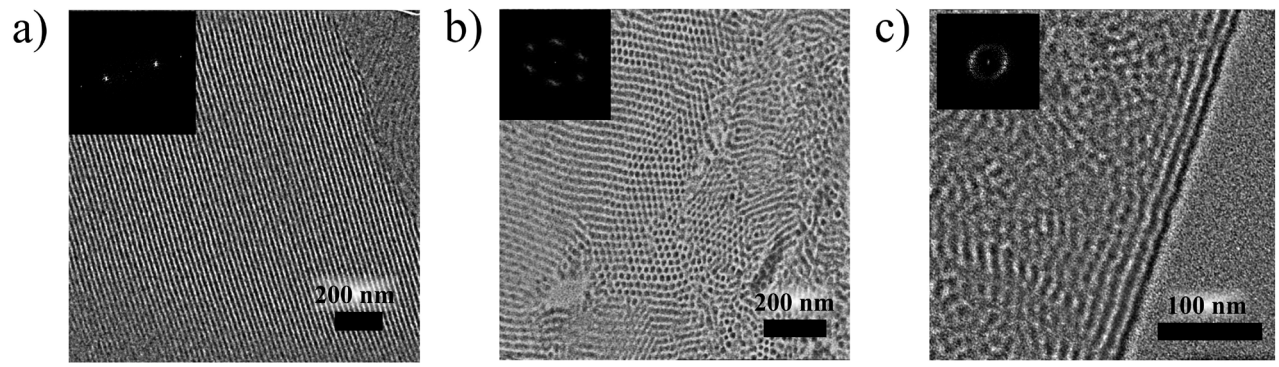

Fig. 4 The TEM images of cross-sections of the (a) pVP_{120}-*b*-pPhM_{40}, (b) pVP_{120}-*b*-pPhM_{100} and (c) pVP_{60}-*b*-pPhM_{40}-*b*-pVP_{60} films. The samples were annealed at 140 °C for 3 h and then stained with iodine for 1 h.

triblock copolymers (Fig. S4†), as it was in the case of the pVP_{60}-*b*-$pPhM_{40}$ diblock copolymer. We suppose that both of these triblock copolymers seem to have too low polymerization degree to form well-organized structures. Judging from the TEM images and the ratio of monomer units, these triblock copolymers are supposed to represent a continuous LC matrix with discrete disordered microphases formed by pVP blocks.

Phase behavior, morphology and fluorescence properties of the LC polymer–QD composites

As the host block copolymers are nematic LC polymers, the prepared LC polymer–QD composites form only nematic LC phase with a marble texture (Fig. 5a). The isotropization temperatures of the composites are almost equal to those of the initial host copolymers (Table 1, Fig. 5b). For example, the isotropization temperature of pVP_{120}-*b*-$pPhM_{100}$ is decreased only by 4 °C after incorporating QDs. Slightly more marked decrease in isotropization temperatures is pointed out in the case of those host block copolymers that do not form clear microphase separated structure. Incorporating QDs does not affect the glass transition temperature of the pPhM block. The glass transition temperature of the pVP block was observed only for the V_{120}-LC_{40} composite and the obtained value is very close to that of the initial host block copolymer.

The important aspect of the morphology of hybrid composite films is the distribution of nanoparticles. Key factors, defining QD distribution within block copolymer-based composite films, are aggregation of QDs and their concentrating into specified microphases of the host block copolymers. Therefore, they should be considered further. Being introduced in amorphous block copolymers containing pVP block QDs concentrate in microphases formed by VP units.[24,35] The same results were obtained for ABA LC triblock copolymers with end pVP blocks in our previous work.[37] From this viewpoint, it is most interesting to consider the morphology of the composites based on host block copolymers that form fine microphase separation structures: pVP_{60}-*b*-$pPhM_{40}$-*b*-pVP_{60}, pVP_{120}-*b*-$pPhM_{40}$ and pVP_{120}-*b*-$pPhM_{100}$. The morphology of the composite films as thin slices were investigated with TEM without staining.

The films of the V_{60}-LC_{40}-V_{60} composite based on pVP_{60}-*b*-$pPhM_{40}$-*b*-pVP_{60} are characterized by the uniform distribution of QDs without any ordering (Fig. 6a and S5†). QDs appear as black dots in the bright field TEM images and as white dots in the dark field TEM image (Fig. S6†) Random nature of the QD distribution appears to be associated with the absence of the long-range order in the microphase separated structure of the initial host block copolymer. Indeed, after staining the composite film with iodine, small areas with the stack of layers can be found (Fig. S7†).

On the contrary, QDs introduced in pVP_{120}-*b*-$pPhM_{40}$ are arranged in layers, as it can be seen from Fig. 6b. The crystalline nature of the observed nanoparticles was confirmed with dark field TEM image (Fig. S8†). The distance between two neighboring QD layers is 17 nm, which is almost the same value, observed for the period of the lamellar structure of the pVP_{120}-*b*-$pPhM_{40}$ film. The same value of period seems to be explained by the low volume fraction of QDs, which could not have affected microphase separated structure appreciably. Indeed, as the density of CdSe is about 6 g cm^{-3}, 10 wt% of QDs incorporated in the composite correspond only to 1.6 vol%. The schematic representation of the structure of this composite is shown in Fig. 7a. Note that despite the presence of clear long-range order of QD layers, the composite film looks less ordered than the film of the initial host block copolymer. The presence of QDs is likely to make some difficulties for self-assembling PhM and VP layers due to extra interaction between pVP blocks.

More pronounced influence of QDs on self-assembling host block copolymer was observed for the V_{120}-LC_{100} composite based on pVP_{120}-*b*-$pPhM_{100}$. The cylindrical structure is supposed to be formed in this composite because QDs change the volume fraction of pVP block only insignificantly. In this case, hexagonal packing of cylinders, which is typical of the host block copolymer, was lost and only disordered cylinders are present in the composite film (Fig. 6c). Some kind of arrangement of cylinders can be seen near the substrate surface but in the bulk the ordering has only a local character. These facts are proved by the corresponding FFT images (Fig. 6c, insets). The inner structure of the composite may be presented as cylinders filled with QDs and immersed in LC matrix (Fig. 7b). Note that

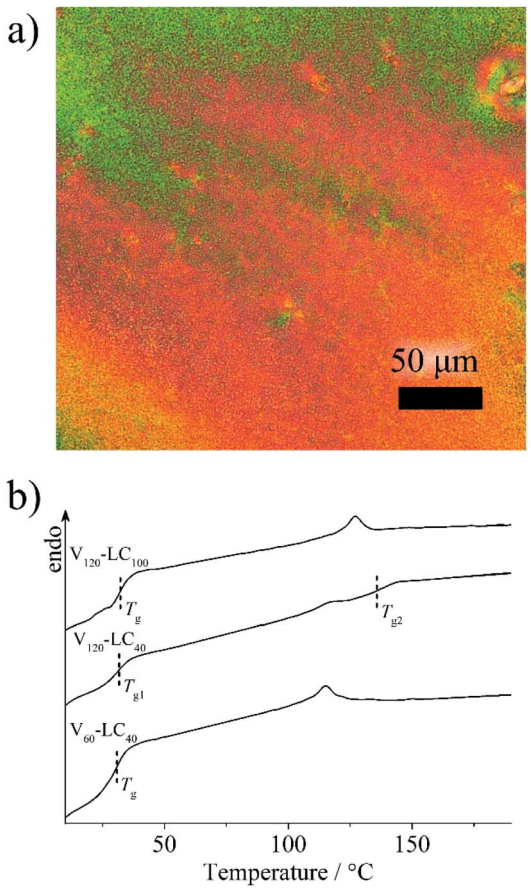

Fig. 5 (a) The POM image of the composite based on pVP_{120}-*b*-$pPhM_{100}$ and (b) DSC curves of the composites based on the LC diblock copolymers.

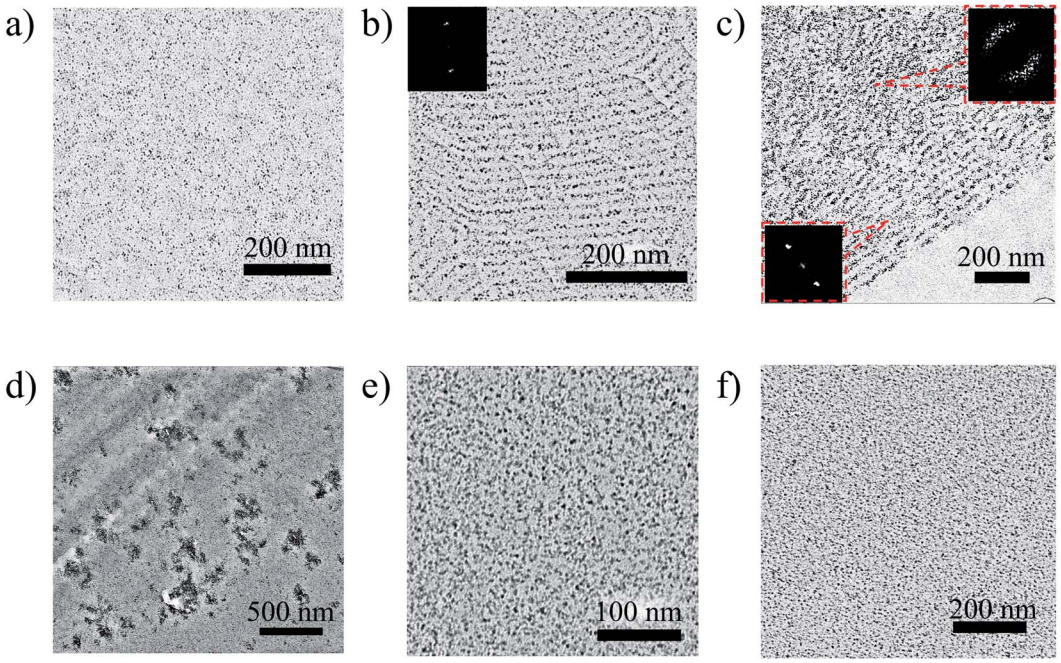

Fig. 6 TEM images of the LC polymer–QD composites: (a) V_{60}-LC_{40}-V_{60}, (b) V_{120}-LC_{40}, (c) V_{120}-LC_{100}, (d) V_{20}-LC_{40}-V_{20}, (e) LC_{20}-V_{40}-LC_{20}, (f) V_{60}-LC_{40}.

the orientation of cylinders can be improved by the orientation of the nematic LC matrix of this composite under external fields. This research is being carried out in our laboratory.

All three composites described above display the absence of QD aggregates indicating that pVP_{60}-*b*-$pPhM_{40}$-*b*-pVP_{60}, pVP_{120}-*b*-$pPhM_{40}$, pVP_{120}-*b*-$pPhM_{100}$ can efficiently stabilize QDs. Contrary to these composites, obvious aggregates of QDs were observed for the V_{20}-LC_{40}-V_{20} film based on pVP_{20}-*b*-$pPhM_{40}$-*b*-pVP_{20} (Fig. 6d). This difference may be explained with relatively short length of pVP_{20}-*b*-$pPhM_{40}$-*b*-pVP_{20} macromolecules, which prefer to connect neighboring QDs than to form loops on the surface of QDs.

This suggestion is confirmed by incorporating QDs into the $pPhM_{20}$-*b*-pVP_{40}-*b*-$pPhM_{20}$ triblock copolymer and the pVP_{60}-*b*-$pPhM_{40}$ diblock copolymer. These block copolymers have the monomer ratio and length of the polymer chain similar to pVP_{20}-*b*-$pPhM_{40}$-*b*-pVP_{20} but they cannot bind two QDs due to their chemical structure. As seen from Fig. 6e, f and S9,† $pPhM_{20}$-*b*-pVP_{40}-*b*-$pPhM_{20}$ and pVP_{60}-*b*-$pPhM_{40}$ provide the uniform distribution of QDs without any aggregates. Therefore, the alteration of the length of the constituent blocks and their location in the macromolecule of a host block copolymer allow the aggregation of QDs to be adjusted.

In the case of VLC-1 and VLC-2, TEM observation shows the uniform distribution of QDs without any aggregation indicating good compatibility between QDs and random copolymers (Fig. S10†). However, VLC-1 and VLC-2 do not display the formation of LC phase similar to the host random copolymers. Hence, the p(VP_{50}-*r*-$pPhM_{50}$) and p(VP_{50}-*r*-$pPhM_{50}$) should not be examined as a suitable polymer matrix for the preparation of LC polymer–QD composites.

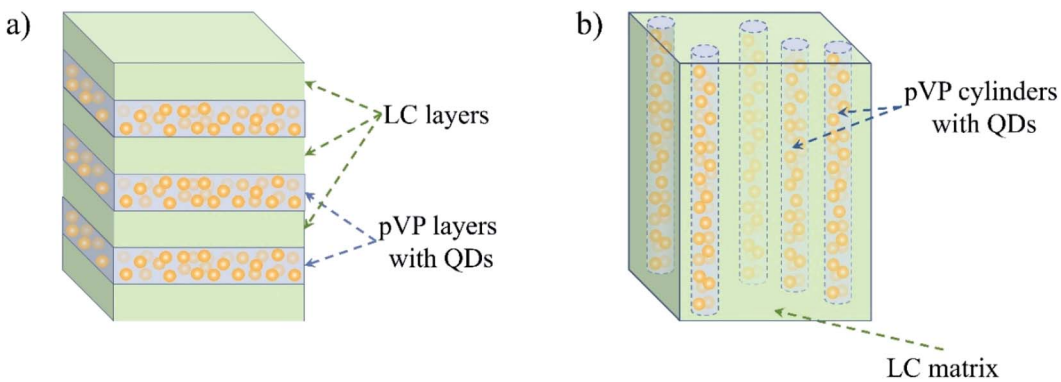

Fig. 7 The schematic representation of the QD distribution in composite films based on (a) pVP_{120}-*b*-$pPhM_{40}$ and (b) pVP_{120}-*b*-$pPhM_{100}$.

The films of the obtained LC polymer–QD composites are characterized by bright and uniform fluorescence in the red region of the visible spectrum (Fig. 8a). Fluorescence spectra of all the composite films except the V_{20}-LC_{40}-V_{20} film have the same feature. As an example, fluorescence spectra of V_{60}-LC_{40}-V_{60} and V_{120}-LC_{40} are shown in Fig. 8b. Fluorescence peaks of these composites are located at 582 nm and match with the spectra of their solutions in $CHCl_3$ (Fig. S11†) confirming the absence of QD aggregates in films of these composites. The fluorescence spectrum of the V_{20}-LC_{40}-V_{20} composite is red-shifted indicating the aggregation of QDs.[48] This fact conforms to TEM observations that show the presence of aggregated QDs in the films of this composite (Fig. 6d). Note that fluorescence spectra of the composites are slightly blue shifted in comparison with that of the pyridine solution of QDs capped with pyridine. This shift is supposed to be associated with higher refractive index of the LC block copolymer matrices than that of pyridine.[49,50]

To sum up, the microphase separated structure of the studied LC block copolymers allows preserving the unique properties of QDs and LC phase due to nanoscale segregation. In other words, the LC polymer–QD composites under study possess intrinsic heterogeneity but it is nanoscale heterogeneity, which can be finely programmed by the chemical structure of a host block copolymer. Because of a nanoscale character, such heterogeneity will not induce undesirable optical phenomena, for instance, light scattering. On the contrary, LC random copolymers or homopolymers are devoid of this potentiality producing composites with the spontaneous QD distribution.

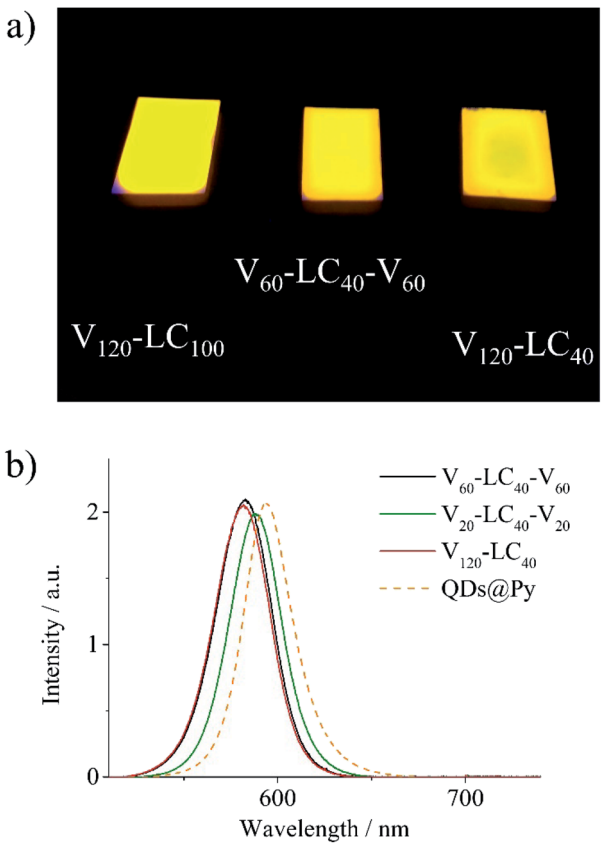

Fig. 8 (a) Photo of the composite films under UV irradiation (λ = 365 nm, I = 1 mW cm^{-2}) and (b) fluorescence spectra of composites films and the pyridine solution of CdSe/ZnS QDs capped with pyridine (QDs@Py).

Experimental

Materials and composite preparation

Chloroform, pyridine, methanol, ethyl ether, ethyl acetate, dimethylformamide (DMF), hexane, 4-vinylpyridine and 2-cyano-2-propyl dodecyl trithiocarbonate (CPDDTC) were purchased from Aldrich. Chloroform was passed through aluminum oxide and distilled. Pyridine was dried over KOH and distilled over CaH_2. CdSe/ZnS quantum dots (QDs) of approximately 5 nm in diameter covered with oleylamine and surrounded by TOPO matrix were synthesized according to the previous report.[43] The LC di and triblock copolymers as well as the random copolymers were synthesized by reversible addition–fragmentation transfer (RAFT) polymerization as described previously (Scheme S1†).[39] The controlled synthesis of copolymers was performed using three different RAFT agents, namely *S*,*S*′-bis(methyl-2-isobutyrate)trithiocarbonate[51] for the ABA block copolymers, commercially available CPDDTC for the diblock copolymers and random copolymers, and a specially designed RAFT agent[40] (Fig. S1b†) for BAB triblock copolymer. As example, the synthesis of pVP_{60}-*b*-$pPhM_{40}$-*b*-pVP_{60} is briefly described in the ESI.†

Ligand exchange technique: the replacement of oleylamine by pyridine

The substitution of oleylamine (OLA) QD ligands for pyridine was done according to the ligand exchange procedure reported earlier.[52] First, QDs were purified from the TOPO matrix by three precipitation/redissolution cycles using chloroform and methanol as the solvent and non-solvent, respectively. Then, the 100 mg portion of QDs was dispersed in 20 ml of anhydrous pyridine and the mixture was placed in an ampoule and purged with argon for 40 min. The ampoule was sealed and heated to 90 °C for 24 h. After that, the reaction ampoule was cooled to room temperature and opened, the solution of ligand-exchanged QDs was precipitated with hexane. The precipitate was collected by centrifugation, washed with an excess of hexane and dried under vacuum. The described procedure was repeated three times to achieve the maximum possible degree of OLA replacement by pyridine. Finally, QDs were dissolved in pyridine and stored as a solution under argon atmosphere at 0 °C.

Ligand exchange technique: the replacement of pyridine by triblock copolymer

The typical procedure of LC block copolymer–QD composite fabrication is shown on the example of V_{60}-LC_{40}-V_{60} sample (see Table 1 in the Results and Discussion section). A portion of QDs solution in pyridine described in the above containing 5.2 mg of

QDs and dispersed in pyridine (150 μl) was added to 47.4 mg of pVP_{60}-*b*-$pPhM_{40}$-*b*-pVP_{60} dissolved in chloroform (1 ml). Then the resulting mixture was thoroughly stirred for 3 h and the solvents were removed under reduced pressure. The obtained solid product was dispersed in 1 ml of chloroform and dried under reduced pressure again. This procedure was repeated five times in order to obtain the final V_{60}-LC_{40}-V_{60} composite.

Measurements

Polarizing optical microscopic (POM) observations were conducted on an Axio Vert. A1 (Carl Zeiss) microscope equipped with a CCD camera and a hot stage. Fluorescence microscopy observations were performed using Micromed 3 LUM microscope (LOMO).

The phase transition temperatures of the polymers were studied by differential scanning calorimetry (DSC) using a PerkinElmer DSC-7 thermal analyzer at the scanning rate of 10 K min^{-1}. The samples were prepared as 10–20 mg pellets. Prior to the measurements, the samples were heated above the isotropic melt point to remove thermal history.

TEM images were taken with a LEO 912 AB Omega transmission electron microscope (Carl Zeiss) operating at an accelerating voltage of 100 kV. TEM specimen were prepared according to the following procedure. The dispersion of composite in chloroform were drop-casted onto a PET substrate, and the obtained films were annealed at 140 °C for 3 h. Then, the annealed samples were embedded in an epoxy resin and cured overnight. The sample was subsequently microtomed to a thickness of about 50 nm using a Reichert-Gung ultramicrotome with a diamond knife (Diatome) at room temperature. The microtomed sections floating in water were placed on copper TEM grids and stained with iodine for 1 h.

Fluorescence spectra were recorded on an M266 automated monochromator/spectrograph (SOLAR Laser Systems, Belarus) equipped with a CCD detector U2C-16H7317 (Ormins, Belarus) and a homemade light-collecting inverted system using a 100×/0.80 MPLAPON lens (Olympus, Japan) and a homemade confocal unit with two 100 mm objective lenses. Excitation light was cut off by Semrock 488 nm RazorEdge® ultrasteep longpass edge filters (Semrock, USA). Fluorescence of QDs was excited by a KLM-473/h-150 laser (Plazma, Russia) operating at the wavelength of 473 nm. An incident light intensity was equal to 50 mW cm^{-2} as measured with a LaserMate-Q (Coherent) intensity meter.

The molecular-mass characteristics of the polymers were analyzed by GPC in DMF containing 0.1 wt% of LiBr at 50 °C on a PolymerLabs GPC-120 chromatograph equipped with two columns PLgel 5 μm MIXED B (M= (5×10^2) to (1×10^7)) and a differential refractometer. PMMA standards were used for calibration.

^{1}H NMR spectra of the QD-polymer composites in the form of 3% solutions in $CDCl_3$ were recorded on a Bruker DRX500 instrument. The infrared spectra were measured on the Thermo Nicolet IR200 FTIR spectrometer using 150 scans at the resolution of 2 cm^{-1}. The samples were drop-casted on KBr plates and dried overnight at room temperature.

Conclusions

We have prepared and studied a series of hybrid fluorescence LC polymer–QD composites based on CdSe/ZnS QDs and host LC block copolymers. The host block copolymers consist of phenyl benzoate LC blocks and poly(4-vinylpyridine) blocks, which are responsible for compatibility between QDs and a host polymer matrix. The content of QDs in the obtained composites was fixed (10 wt%) but the molecular architecture of host block copolymers was varied. We considered three types of block copolymers including AB diblock copolymers, ABA and BAB triblock copolymers. In spite of high content of QDs, all the composites exhibit nematic LC phase with temperature range which is close to that of the initial host LC block copolymers. It was found out that for host ABA triblock copolymers with end poly(4-vinylpyridine) blocks, QDs form pronounced aggregates when the total polymerization degree of a block copolymer is about 80. In case of a BAB triblock copolymer and ABA triblock copolymer with higher degree of polymerization the uniform distribution of QDs within composite films was observed. The aggregation of QDs can thus be controlled with length of the constituent blocks and their location in the macromolecule of a host LC triblock copolymer. QDs incorporated in diblock copolymers do not form any aggregates as opposed to the host triblock copolymers. Due to well-organized microphase separated structure of the diblock copolymers, QDs are arranged in either lamellar or cylindrical arrays. It should be pointed out that random copolymers turn out to be unsuitable for the preparation of LC polymer–QD composites. These copolymers can stabilize QDs but despite the same monomer ratio as that of block copolymers, they do not form any LC phase. It was shown that all composite films demonstrate bright fluorescence under UV and blue irradiation, with spectral characteristics being virtually the same as those of initial QDs. Thus, the LC block copolymers containing pVP block seem to be an efficient tool for designing LC polymer–QD composites with programmed arrangement of QDs.

Conflicts of interest

There are no conflicts to declare.

Acknowledgements

This study was financially supported by the Russian Science Foundation (Grant No. 19-73-00058).

References

1 S. H. Cho, J. Sung, I. Hwang, R. H. Kim, Y. S. Choi, S. S. Jo, T. W. Lee and C. Park, *Adv. Mater.*, 2012, **24**, 4540–4546.
2 M. A. Najeeb, S. M. Abdullah, F. Aziz, M. I. Azmer, W. Swelm, A. A. Al-Ghamdi, Z. Ahmad, A. Supangat and K. Sulaiman, *RSC Adv.*, 2016, **6**, 23048–23057.

3 P. Ilaiyaraja, P. S. V. Mocherla, T. K. Srinivasan and C. Sudakar, *ACS Appl. Mater. Interfaces*, 2016, **8**, 12456–12465.
4 Q. Ma and X. Su, *Analyst*, 2011, **136**, 4883–4893.
5 C. Zhang, H. Cui, J. Cai, Y. Duan and Y. Liu, *J. Agric. Food Chem.*, 2015, **63**, 4966–4972.
6 Y. Cai, G. Du, G. Gao, J. Chen and J. Fu, *RSC Adv.*, 2016, **6**, 98147–98152.
7 H. Wang, Z. Shao, B. Chen, T. Zhang, F. Wang and H. Zhong, *RSC Adv.*, 2012, **2**, 2675–2677.
8 J. He, H. H. Chen, H. H. Chen, Y. Wang, S.-T. Wu and Y. Dong, *Opt. Express*, 2017, **25**, 12915–12925.
9 J. M. Pietryga, Y.-S. Park, J. Lim, A. F. Fidler, W. K. Bae, S. Brovelli and V. I. Klimov, *Chem. Rev.*, 2016, **116**, 10513–10622.
10 P. Reiss, M. Carrière, C. Lincheneau, L. Vaure and S. Tamang, *Chem. Rev.*, 2016, **116**, 10731–10819.
11 H. Kang, S. Kim, J. H. Oh, H. C. Yoon, J.-H. Jo, H. Yang and Y. R. Do, *Adv. Opt. Mater.*, 2018, **6**, 1701239.
12 H. Y. Kim, D.-E. Yoon, J. Jang, D. C. D. Lee, G.-M. Choi, J. H. Chang, J. Y. Lee, D. C. D. Lee and B.-S. Bae, *J. Am. Chem. Soc.*, 2016, **138**, 16478–16485.
13 J. Yao, P. Ji, B. Wang, H. Wang and S. Chen, *Sens. Actuators, B*, 2018, **254**, 110–119.
14 Y. Zhang, Y. Tian, L.-L. Xu, C.-F. Wang and S. Chen, *Chem. Commun.*, 2015, **51**, 17525–17528.
15 G. A. Shandryuk, E. V. Matukhina, R. B. Vasil'ev, A. Rebrov, G. N. Bondarenko, A. S. Merekalov, A. M. Gas'kov and R. V. Talroze, *Macromolecules*, 2008, **41**, 2178–2185.
16 A. Bobrovsky, K. Mochalov, V. Oleinikov, A. Sukhanova, A. Prudnikau, M. Artemyev, V. Shibaev and I. Nabiev, *Adv. Mater.*, 2012, **24**, 6216–6222.
17 L. Tan, Y. Shi and Y. Chen, *Sol. Energy*, 2016, **129**, 184–191.
18 G. I. Tselikov, G. A. Shandryuk, I. Y. Kutergina, A. M. Shatalova, A. S. Merekalov, V. Y. Timoshenko and R. V. Talroze, *Polym. Sci., Ser. A*, 2014, **56**, 781–785.
19 M. Urbanski, B. Kinkead, T. Hegmann and H.-S. Kitzerow, *Liq. Cryst.*, 2010, **37**, 1151–1156.
20 U. B. Singh, R. Dhar, A. S. Pandey, S. Kumar, R. Dabrowski and M. B. Pandey, *AIP Adv.*, 2014, **4**, 117112.
21 S. Singh, A. Singh, M. Mittal, R. Srivastava, S. Sapra and B. Nandan, *Phys. Chem. Chem. Phys.*, 2019, **21**, 16137–16146.
22 R. B. Cheyne and M. G. Moffitt, *Macromolecules*, 2007, **40**, 2046–2057.
23 L. Chen, C. Zhang, Z. Du, H. Li, L. Zhang and W. Zou, *RSC Adv.*, 2015, **5**, 65184–65191.
24 C.-P. Li, K.-H. Wei and J. Y. Huang, *Angew. Chem., Int. Ed.*, 2006, **45**, 1449–1453.
25 H. Yusuf, W.-G. Kim, D. H. Lee, M. Aloshyna, A. G. Brolo and M. G. Moffitt, *Langmuir*, 2007, **23**, 5251–5254.
26 K. H. Ku, M. P. Kim, K. Paek, J. M. Shin, S. Chung, S. G. Jang, W.-S. Chae, G.-R. Yi and B. J. Kim, *Small*, 2013, **9**, 2667–2672.
27 J. Kwak, W. K. Bae, M. Zorn, H. Woo, H. Yoon, J. Lim, S. W. Kang, S. Weber, H.-J. Butt, R. Zentel, S. Lee, K. Char and C. Lee, *Adv. Mater.*, 2009, **21**, 5022–5026.
28 K. Palaniappan, N. Hundt, P. Sista, H. Nguyen, J. Hao, M. P. Bhatt, Y. Y. Han, E. A. Schmiedel, E. E. Sheina, M. C. Biewer and M. C. Stefan, *J. Polym. Sci., Part A: Polym. Chem.*, 2011, **49**, 1802–1808.
29 Y.-J. Kim, C.-H. Cho, K. Paek, M. Jo, M. Park, N.-E. Lee, Y. Kim, B. J. Kim and E. Lee, *J. Am. Chem. Soc.*, 2014, **136**, 2767–2774.
30 J. N. Cha, M. H. Bartl, M. S. Wong, A. Popitsch, T. J. Deming and G. D. Stucky, *Nano Lett.*, 2003, **3**, 907–911.
31 S. Huang, Y. Chen, S. Ma and H. Yu, *Angew. Chem., Int. Ed.*, 2018, **57**, 12524–12528.
32 H. Yu, *Prog. Polym. Sci.*, 2014, **39**, 781–815.
33 H.-C. Kim, S.-M. Park and W. D. Hinsberg, *Chem. Rev.*, 2010, **110**, 146–177.
34 A. Rahman, P. W. Majewski, G. Doerk, C. T. Black and K. G. Yager, *Nat. Commun.*, 2016, **7**, 13988.
35 S. Singh, P. Samanta, R. Srivastava, A. Horechyy, U. Reuter, M. Stamm, H.-L. Chen and B. Nandan, *Phys. Chem. Chem. Phys.*, 2017, **19**, 27651–27663.
36 M. Zorn, W. K. Bae, J. Kwak, H. Lee, C. Lee, R. Zentel and K. Char, *ACS Nano*, 2009, **3**, 1063–1068.
37 M. Bugakov, N. Boiko, P. Samokhvalov, X. Zhu, M. Möller and V. Shibaev, *J. Mater. Chem. C*, 2019, **7**, 4326–4331.
38 N. I. Boiko, V. P. Shibaev and M. Kozlovsky, *J. Polym. Sci., Part B: Polym. Phys.*, 2005, **43**, 2352–2360.
39 M. A. Bugakov, N. I. Boiko, E. V. Chernikova, S. S. Abramchuk and V. P. Shibaev, *Polym. Sci., Ser. C*, 2018, **60**, 3–13.
40 N. A. Cortez-Lemus, V. Baldenebro, A. Zizumbo-Lopez and A. Licea-Claverie, *Macromol. Symp.*, 2013, **325–326**, 47–55.
41 E. V. Sivtsov, A. I. Gostev, E. V. Parilova, A. V. Dobrodumov and E. V. Chernikova, *Polym. Sci., Ser. C*, 2015, **57**, 110–119.
42 B. L. Funt and E. A. Ogryzlo, *J. Polym. Sci.*, 1957, **25**, 279–284.
43 V. Krivenkov, P. Samokhvalov, M. Zvaigzne, I. Martynov, A. Chistyakov and I. Nabiev, *J. Phys. Chem. C*, 2018, **122**, 15761–15771.
44 S.-Y. Park, W.-H. Sul and Y.-J. Chang, *Macromolecules*, 2007, **40**, 3757–3764.
45 H. Yu, T. Kobayashi and H. Yang, *Adv. Mater.*, 2011, **23**, 3337–3344.
46 V. Castelletto and I. W. Hamley, *Curr. Opin. Solid State Mater. Sci.*, 2004, **8**, 426–438.
47 A. M. Mayes, R. D. Johnson, T. P. Russell, S. D. Smith, S. K. Satija and C. F. Majkrzak, *Macromolecules*, 1993, **26**, 1047–1052.
48 X. Gong, C. Y. Tang, L. Pan, Z. Hao, C. P. Tsui and J. Liu, *Composites, Part B*, 2013, **55**, 234–239.
49 Y. Li, E. C. Y. Liu, N. Pickett, P. J. Skabara, S. S. Cummins, S. Ryley, A. J. Sutherland and P. O'Brien, *J. Mater. Chem.*, 2005, **15**, 1238–1243.
50 J. Schmitt, P. Mächtle, D. Eck, H. Möhwald and C. A. Helm, *Langmuir*, 1999, **15**, 3256–3266.
51 E. V. Chernikova, Z. A. Poteryaeva, S. S. Belyaev, I. E. Nifant'ev, A. V. Shlyakhtin, Y. V. Kostina, A. S. Cherevan', M. N. Efimov, G. N. Bondarenko and E. V. Sivtsov, *Polym. Sci., Ser. B*, 2011, **53**, 391–403.
52 Q. Li, B. Sun, I. a. Kinloch, D. Zhi, H. Sirringhaus and A. H. Windle, *Chem. Mater.*, 2006, **18**, 164–168.